Jordan Journal of Civil Engineering, Volume **10**, No. **1**, **2016**

Nonlinear Analysis of Reinforced Concrete Beams Strengthened by Prestressed CFRP Sheets under Static Loads

Qassim M. Shaker [1] ***and Hayder H. H. Kamonna*** [2]

[1] University of Kufa, College of Engineering, Civil Engineering Department. E-Mail: qasimm.alabbasi@uokufa.edu.iq
[2] University of Kufa, College of Engineering, Civil Engineering Department. E-Mail: kamonnahh@yahoo.com

ABSTRACT

A nonlinear finite element study has been conducted to evaluate the efficiency of the technique of strengthening reinforced concrete beams under static loads. No time-dependent effects (creep and shrinkage... etc.) are considered in this work. This concept is based on prestressing of CFRP sheets.

In this research program, four reinforced concrete beams were tested to investigate the feasibility of such concept for flexural strengthening. One of the beams was retrofitted with non-prestressed CFRP sheet which was used as the control beam. The rest were retrofitted with prestressed CFRP sheet with three levels of prestressing. The static load was applied at the instant of full prestress load application. Prestress losses were ignored here.

CFRP sheets have been simulated using two types of element (SHELL41 and LINK8). Prestressing effects have been represented using two models; the application as axial load and initial axial strain. The results showed that there is a good enhancement in performance of the beams strengthened using the prestressing technique in terms of the cracking loads and deflection occurs at such level of loading. The application of prestressing forces of 9 kN, 16 kN and 22 kN, was found to increase the cracking load by 57%, 106% and 170%, respectively.

KEYWORDS: Carbon fiber, Reinforced concrete, Nonlinear analysis, Finite element, Prestress.

INTRODUCTION

The aging or deterioration of existing reinforced concrete structures is one of the major problems that civil engineers have to face. If strength of a structure is (or becomes) insufficient to maintain its service loads, strengthening (or upgrading) becomes necessary. The first use of external steel tendons in rehabilitation and upgrading area backs already to the 1950s. To date, externally fixed steel plates/bars have been used to strengthen concrete members (Nordin, 2003).

However, there may be a problem with corrosion in steel that forces the use of steel protection on the external tendons (ACI-440, 2007). This drawback has been overcome using FRP materials. Thus, research in this area has been conducted since the 1970s (Clarke, 1993).

The main advantages of the externally bonded FRP system include: light weight, being noncorrosive and high tensile strength of the FRP. These in turn provide a more flexible and economical technique than traditional steel-plate/jacket techniques, particularly in the areas with limited access (Nordin, 2003; ACI-440, 2007). Other advantages of using FRPs are: improved fire resistance, reduced risk of freeze-and-thaw and damage which reduce construction period (Hollaway

Accepted for Publication on 22/10/2014.

and Leeming, 2001).

Most of the investigations used the non-prestressed method by gluing or bolting the FRPs to the members' surfaces. But, this method has a common problem of de-bonding or de-lamination. Hence, it could not fully utilize the full tensile strength of the FRP, nor it could increase the members' flexural stiffness; being therefore not economical (Shang et al., 2005).

Since non-prestressed FRP sheets support only the additional live loads applied to a structure and can not support existing dead loads, the strengthened or rehabilitated beam may violate the deflection requirements. In other words, beams strengthened with FRP sheets can not deal with the existing deflections caused by the dead load. With addition to live loads, the total deflection may be too large. The prestressed plates will cause a camber after the prestress is transferred to the reinforced concrete members. This phenomenon will help solve the deflection problem. In some cases, the camber can give the beams larger load-carrying capacities. This means that prestressing could be applied, strengthening material can be better utilized and better strengthening results can be achieved. Therefore, the use of FRP as prestressed reinforcement for concrete structure has increased over the past two decades (Nordin, 2003).

Research has shown that small prestress loss (5%-7%) may be experienced due to long-term corrosion in the composite (Nordin, 2003). However, the linear elastic behavior of the FRP material up to failure requires special design considerations to ensure a safe construction due to possible brittle failure (Gangarao, 2007). External prestressed cables of CFRP materials have shown to be an alternative to installing steel plates or external prestressing cables (Peter and Kanstad, 2002). Good durability properties and a first-rate behavior in creep and relaxation have given very good results so far (Hollaway, 2001).

Material Constitutive Relations

Concrete in Compression

The behavior of concrete in compression can be simulated in ANSYS program by an elasto-plastic hardening model followed by a perfectly plastic response which is terminated at the onset of crushing.

The compressive uniaxial stress-strain curve (Fig. 1) for concrete model was obtained using the following equations to compute the multi-linear isotropic stress-strain curve for the concrete (Anthony, 2001).

$$f_c = \varepsilon \; E_c \qquad for \qquad 0 \le \varepsilon \le \varepsilon_1 \tag{1}$$

$$f_c = \frac{\varepsilon E_c}{1+(\varepsilon/\varepsilon_0)^2} \qquad for \qquad \varepsilon_1 \le \varepsilon \le \varepsilon_\circ \tag{2}$$

$$f_c = f_c^{'} \qquad for \qquad \varepsilon_\circ \le \varepsilon \le \varepsilon_{cu} \tag{3}$$

and

$$\varepsilon_1 = 0.3 f_c^{'}/(E_c) \text{ (Hooke's law)} \tag{4}$$

$$\varepsilon_\circ = 2 f_c^{'}/(E_c) \tag{5}$$

where

f_c = stress at any strain ε (MPa),

ε = strain at stress f_c,

ε_o = strain at ultimate compressive stress $f`_c$ and

$E_c = 4750\sqrt{f_c'}$ concrete elastic modulus (MPa).

Tensile Behavior of Concrete

Until the crack, initial tangent modulus E_c is used to find the maximum positive (tensile) stress. After concrete cracking takes place, a smeared crack model is used to represent the discontinuous macro-crack behavior. This cracked concrete can still carry some tensile stress perpendicular to the crack, which is termed tension stiffening. The tension stiffening factor (α_m), Fig. 2, was assumed 0.6. In this work, a simple descending line is used to model this tension stiffening phenomenon.

Modeling of Crack

In concrete, when the tensile stress in the principal direction exceeds the tensile strength, $f`_t$, of concrete,

the tensile failure would occur (Desai et al., 2002). After the crack forms, both normal and shear stiffness are reduced.

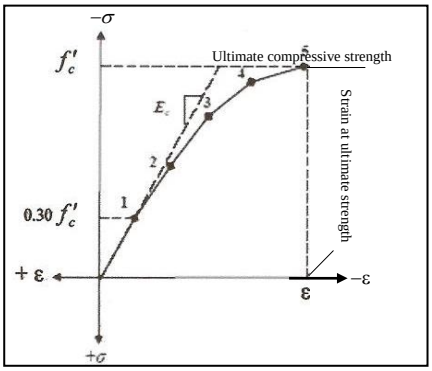

Figure (1): Uniaxial stress-strain curve for concrete (Anthony, 2001)

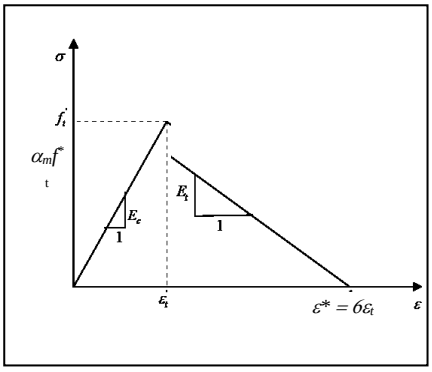

Figure (2): Tension stiffening model (Desai et al., 2002)

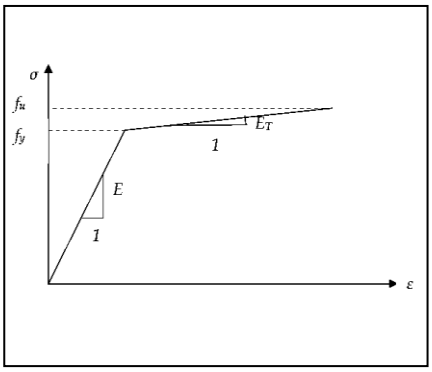

Figure (3): Uniaxial stress-strain relation for steel (SAS, 2005)

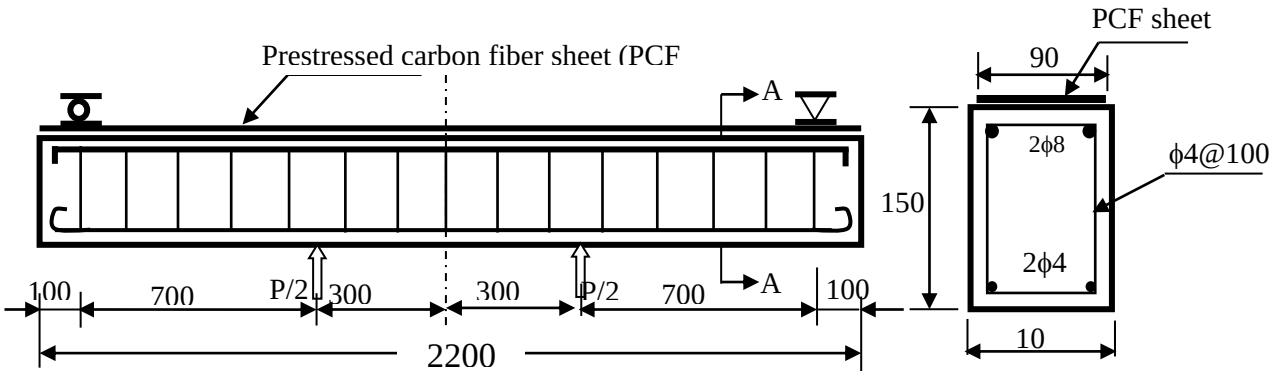

Figure (4): Beam details and loading arrangement (Shang et al., 2005)

Table 1. Test results of material properties (Shang et al., 2005)

Material	Strength (MPa)	Modulus of elasticity (MPa)
CFRP sheet tensile strength	2941	207200
Longitudinal steel bars (8 mm diameter) tensile strength	309.9	224500
Steel stirrups (cold-drawn steel) yield strength	595	201200
Concrete cube compressive strength	24.9	29700

Steel Reinforcing Bars

The stress-strain curve of the reinforcing bars is assumed to be elastic up to the steel yield stress (f_y) followed by linear hardening up to the steel ultimate strength (f_u) as shown in Fig. 3. The dowel action of the reinforcing steel is neglected and the bond between

steel and concrete is assumed to remain perfect.

Experimental Program

Five beams, four with prestressed-CFRP sheet and one non-prestressed-CFRP were constructed and tested by Shang et al. Two of them were tested at the same level of prestress (16 kN) which yielded similar behavior (so, in the present work only one of them is considered). All beams have the same dimensions of 100 × 150 × 2200 mm (width × depth × length) as shown in Fig. 4. The span of the beams was 2000 mm. The steel reinforcement ratio was 0.67%. The CFRP sheet used was 90 mm wide with an average thickness of 0.167 mm. One layer of CFRP was applied to the reinforced concrete beams. The properties of the concrete and steel obtained from tests are summarized in Table (1). Also, prestressing details for all beams are shown in Table (2).

Table 2. Prestressing details (Shang et al., 2005)

Beam ID	Prestress (kN)	CFRP initial stress due to prestressing (MPa)	Prestressing level (%of FRP ultimate strength)	CFRP initial strain due to prestressing ($\times 10^{-6}$)
B1	0	0	0	0
B2	9.0	588	20	3300
B3	16.0	1046	35	6000
B4	22.0	1438	50	8400

Table 3. Real constant typical model

Real constant set	Element type		Real constants		
1 (concrete)	SOLID65	Material number, Volume ratio and orientation angles	for rebar 1	for rebar 2	for rebar 3
			0	0	0
2 (main reinforcement)	LINK8	Cross-sec. area (mm^2)	50.2655		
		Initial strain (mm/mm)	0		
3 (stirrups)	LINK8	Cross-sec. area (mm^2)	12.5664		
		Initial strain (mm/mm)	0		
4 (CFRP sheets)	SHELL41	Thickness (mm)	0.167		
		Elem. x-axis rotation	0		
	LINK8	Cross-sec. area (mm^2)	7.515		
		Initial strain (mm/mm)	0		

ANSYS Finite Element Model

The FEA calibration study included modeling reinforced concrete beams prestressed with CFRP sheets.

Element Types

An 8-noded solid element, **SOLID65** is used to model the concrete. Steel reinforcement and CFRP sheets are modeled using **LINK8** elements. Two nodes are required for this element. Loading and support plates are modeled using the 8-noded solid element **SOLID45.** The CFRP sheet has been modeled using the 4-noded **SHELL41** element. It is a 3-D element having membrane (in-plane) stiffness but no bending

(out-of-plane) stiffness. Each node of all adopted elements has three degrees of freedom, translations in *x*, *y*, and *z* directions (SAS, 2005).

Table 4. Material models for this study

Material Model Number	**Element Type**	**Material Properties**						
1	SOLID65	**Linear Isotropic**		**Multilinear Isotropic**			**Concrete**	
		EX	29700 MPa	Point	strain	Stress(MPa)	ShrCf-Op	0.2
		PRXY	0.2	Point1	0.00022896	6.8	ShrCf-Cl	0.6
				Point2	0.0005	11.11	UnTensS	2.49
				Point3	0.00075	15.639	UnComp	24.9
				Point4	0.001	19.196	BiCompS	0
				Point5	0.00125	21.771	HydroPrs	0
				Point6	0.0015	23.468	BiCompS	0
				Point7	0.00175	24.441	UnTensrFac	0
				Point8	0.002	24.7		
				Point9	0.0035	24.9	St TenC	0.6
2	LINK8	Linear Isotropic		Bilinear Isotropic				
		EX	2.245e5 MPa	Yield Stress	309.9 MPa			
		PRXY	0.3	Tang Mod	224.5 MPa			
3	LINK8	Linear Isotropic		Bilinear Isotropic				
		EX	2.012e5 MPa	Yield Stress	595 MPa			
		PRXY	0.3	Tang Mod	201.2 MPa			
4	SHELL41	Linear Isotropic		Bilinear Isotropic				
		EX	2.072e5 MPa	Yield Stress	2941			
		PRXY	0.3	Tang Mod	207.2			
5	SOLID45	Linear Isotropic						
		EX	2.072e5 MPa					
		PRXY	0.3					

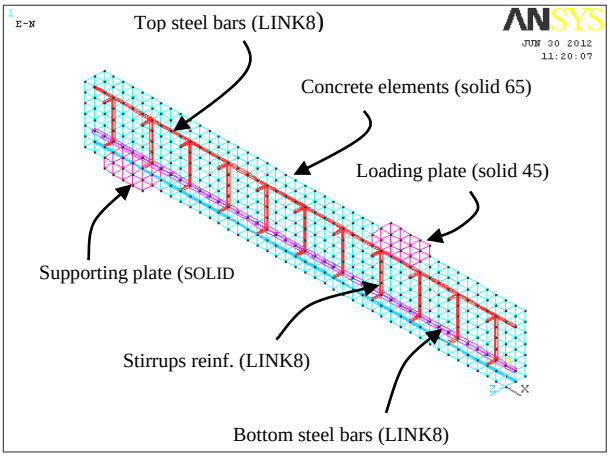

Figure (5): Mesh of concrete, steel plate and steel support

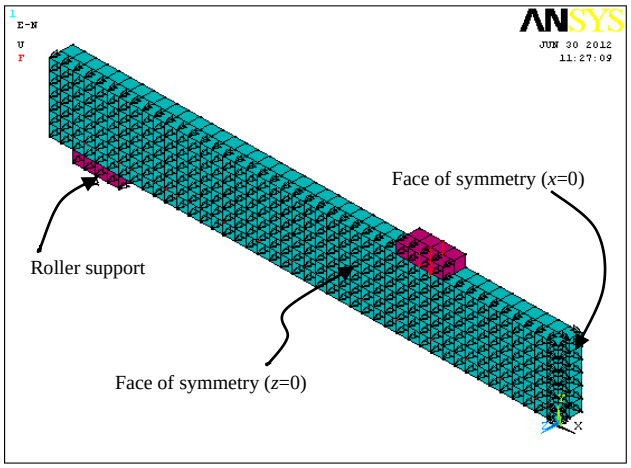

Figure (6): Boundary conditions

Real Constants

The real constants needed for this model are shown in Table 3. It can be noted that the individual elements may contain different real constants. No real constant set exists for the SOLID45 element.

Real constant set 1 is used for the SOLID65 element. It requires real constants for rebar assuming a smeared model, then, values for material number, volume ratio and orientation angles for three directions may be entered. In the present study, the steel in beams is modeled using discrete model. Therefore, a value of zero was entered for all real constants which turned the smeared reinforcement capability of the SOLID65 element off.

Real constant sets 2 and 3 are defined for the LINK8 element. Set 4 refers to the CFRP sheets modeled using SHELL41 element. Also, an alternative LINK8 element has been assumed to study the difference between the two models.

Material Properties

Parameters used to define the material models are listed in Table (4). It is clear that there are multiple parts of the material model for each element. The first material model refers to the SOLID65 element. It requires linear isotropic and multi-linear isotropic material properties to properly model concrete. The multi-linear isotropic material uses the von-Mises failure criterion along with the (William and Warnke, 1974) model to define the failure of the concrete. Material model numbers 2 to 4 refer to the LINK8 and SHELL41 elements which are assumed to be bilinear isotropic material based on the von-Mises failure criterion. Material model number 5 refers to the SOLID45-element, that is modeled as a linear isotropic element.

Modeling Methodology

By taking advantage of the symmetry of the beams, a quarter of the full beams are used for modeling with proper boundary conditions, Fig. 5. However, in this study, perfect bond between materials is assumed. The mesh was set up such that square or rectangular elements were created to obtain good results when using the SOLID65 element (SAS, 2005).

The boundary conditions are shown in Fig. 6. The models adopted in the present work to simulate CFRP sheets are shown in Fig. 7.These are the bar model using LINK8 element and the sheet model using SHELL41 element.

Load-Deflection Relationships

The load-midspan deflection relationships of the tested beams are shown in Figs. 8 to 11. Figures reveal

that the experimental behavior is stiffer than that obtained by numerical analysis. It can be seen that the beams with higher levels of prestress reach their ultimate loads with lesser amount of deformation.

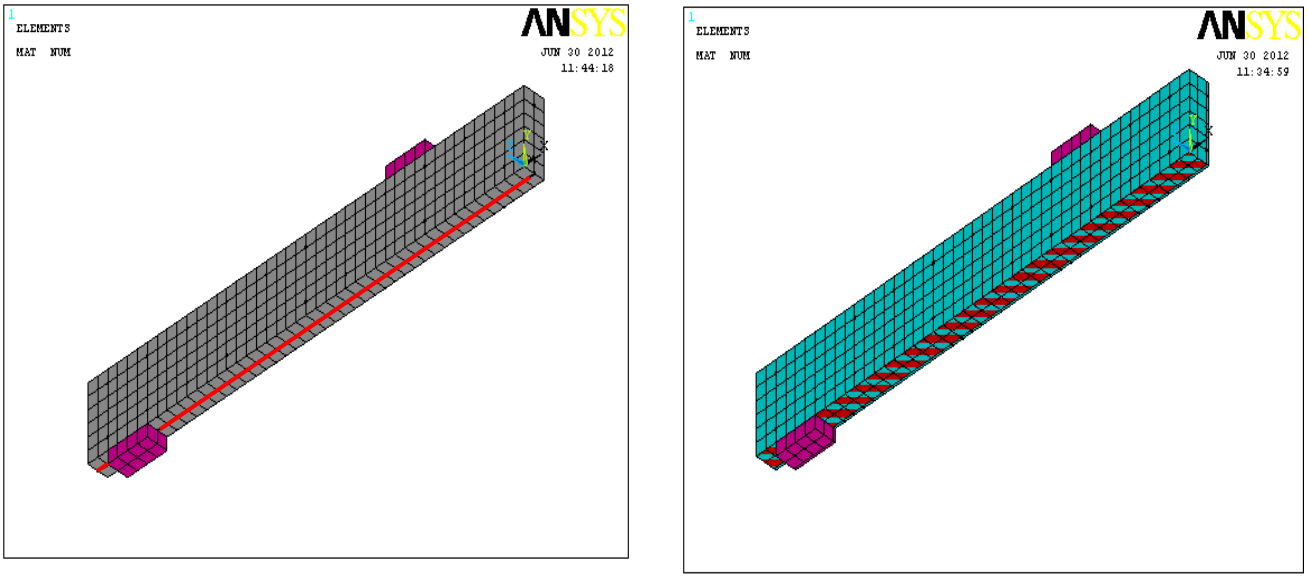

a) Bar model (LINK8 element)

b) Sheet model (SHELL41 element)

Figure (7): CFRP reinforcement modeling

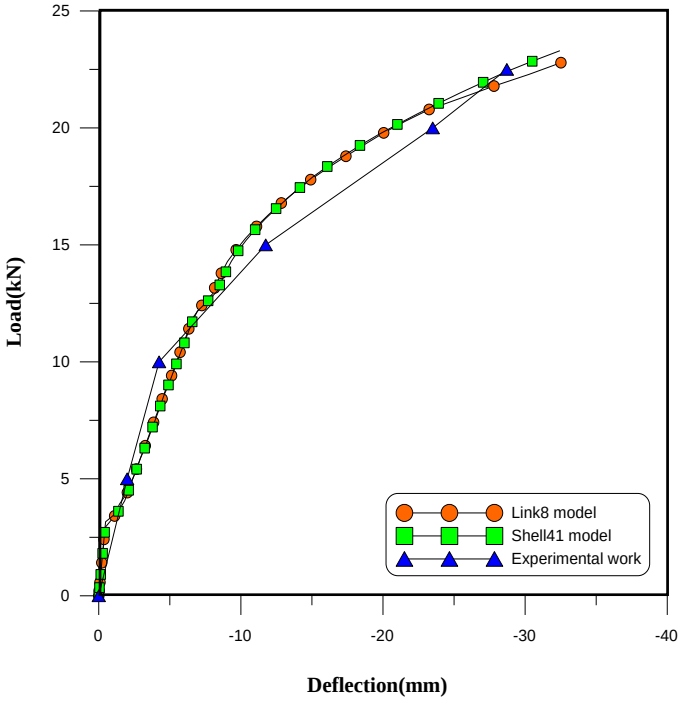

Figure (8): Load - deflection curves for beam B1

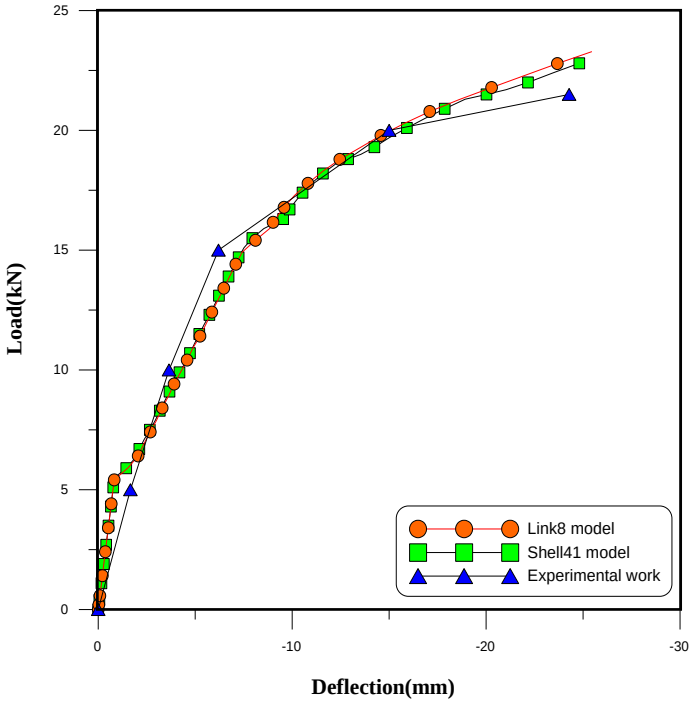

Figure (9): Load - deflection curves for beam B2

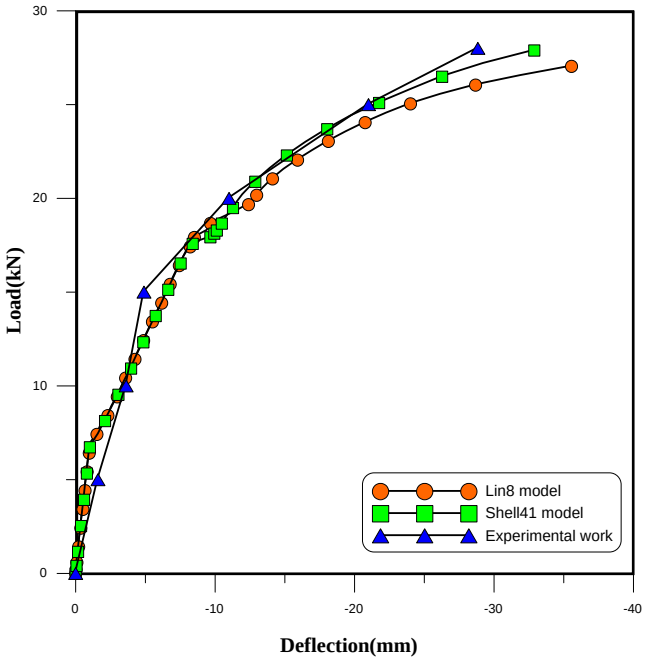

Figure (10): Load-deflection curves for beam B3

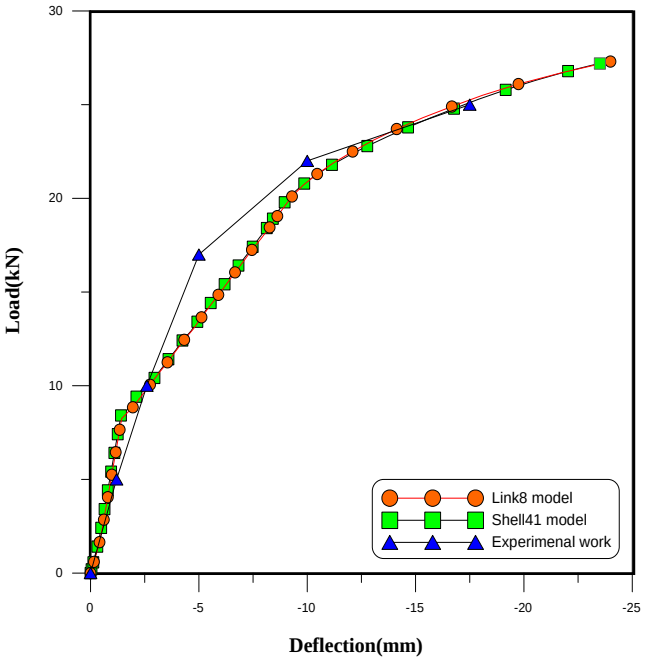

Figure (11): Load-deflection curves for beam B4

In general, good agreement can be seen for most of the path of load-deflection curves for beams B1, B2 and B3, Figs. 8 to 10. For beam B4, this agreement continued up to the instant of carbon sheet cut-off (which occurred experimentally at a load of 25 kN) giving a deflection of 16 mm, Fig. 11. In contrast, the numerical analysis continued beyond this point with an ultimate deflection of 24 mm (no cut-off). This can be attributed to the fact of gradual yielding of SHELL41 element without cut- off and the failure is indicated by the high strain value that results in divergence in the numerical solution (SAS, 2005). The deflection values *versus* cracking loads and ultimate loads for theoretical and experimental results are listed in Table (5).

Table 5. Comparison of deflections, cracking loads and ultimate loads for theoretical and experimental results

Beam no.	*Def. at load 17kN(mm)*		*Ultimate def. mid-span (mm)*		*Cracking load (kN)*		*Ultimate load (kN)*	
	Exp.	*Theor.*	*Exp.*	*Theor.*	*Exp.*	*Theor.*	*Exp.*	*Theor.*
B1	15.65	13.50	28.71	32.00	4.00	3.50	22.50	22.80
B2	9.26	9.30	24.28	25.00	5.00	5.50	21.50	22.40
B3	7.60	7.50	28.84	32.40	8.00	7.20	28.00	28.00
B4	4.70	6.00	16.00	24.00	11.00	9.50	25.00	27.00

It is obvious that with the increase of prestress, there will be some increase in cracking load. Table (5) shows the values of cracking load relative to the non-prestressed beam. It is found that some increase of cracking load has been obtained for beams B2, B3 and B4 which amounted to 57%, 106% and 171%, respectively. This means that the application of prestress results in the development of the stiffness of beam and hence, the advantage of adopting the principle of prestress seems to be clear.

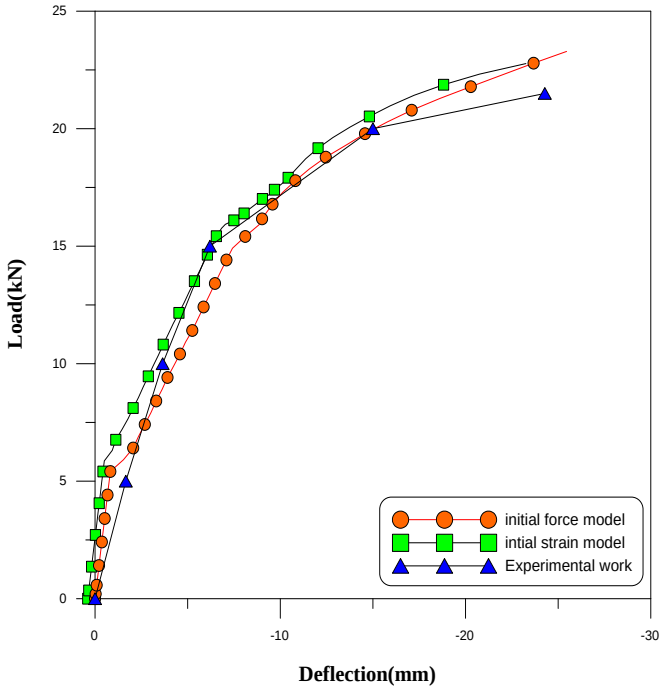

Figure (12): Effect of manner of prestress inclusion on the load –deflection curves for beam B2

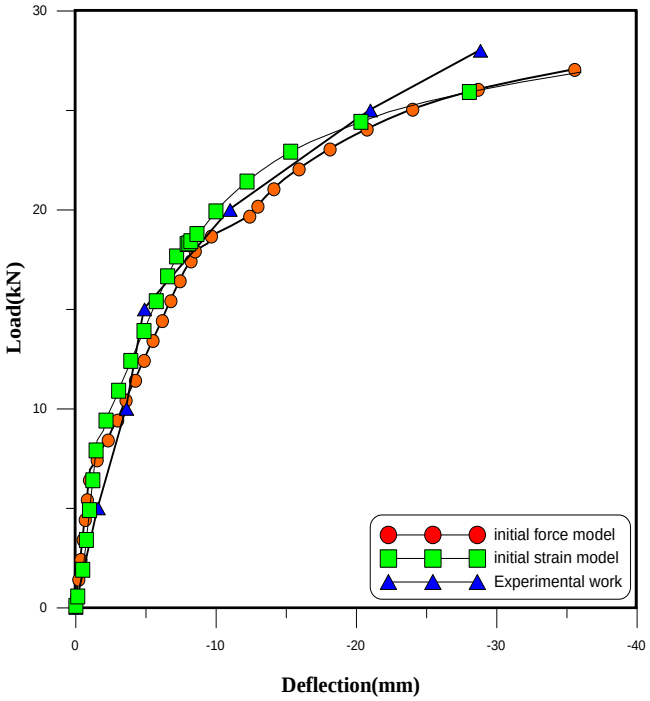

Figure (13): Effect of manner of prestress inclusion on the load –deflection curves for beam B3

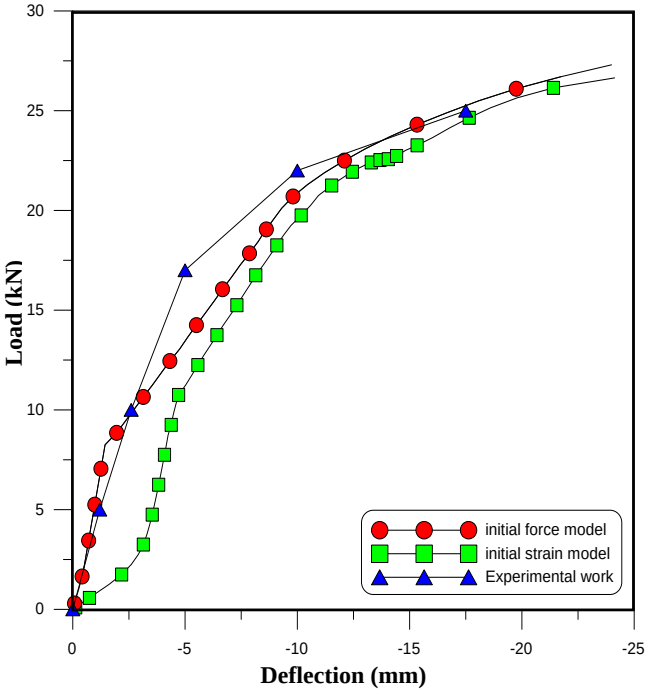

Figure (14): Effect of manner of prestress inclusion on the load-deflection curves for beam B4

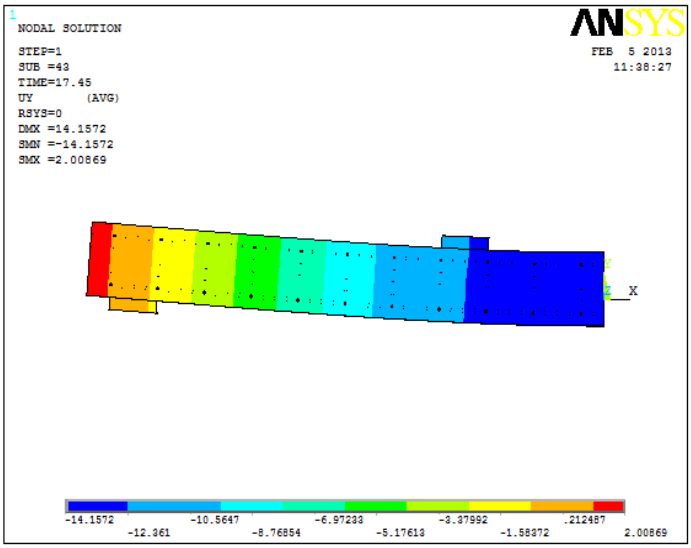

Figure (15): Deflection at load = 17.45 kN for B1

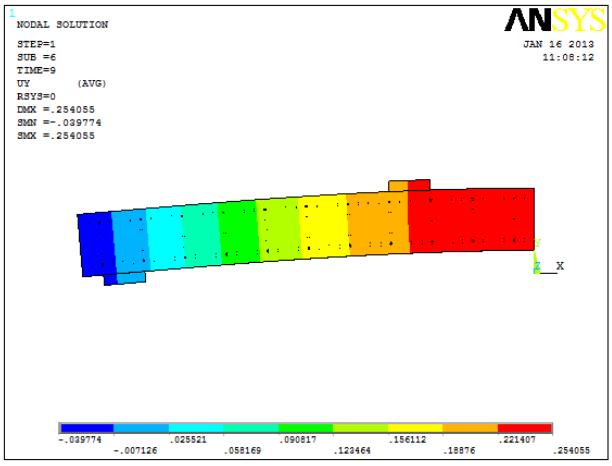

Figure (16): Camber for beam B2

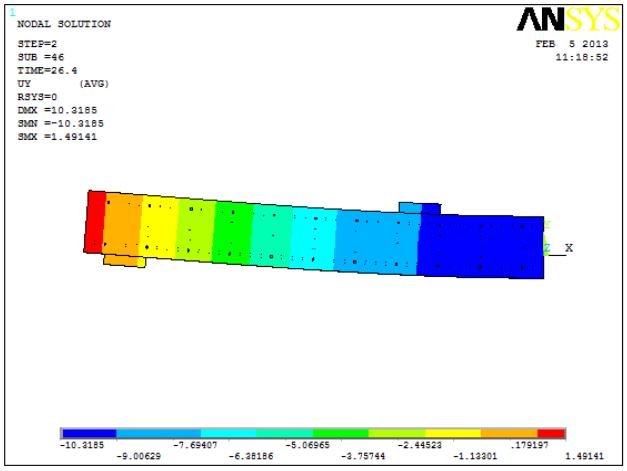

Figure (17): Deflection at load = 17.45 kN for B2

It can also be seen that no significant difference was found in the ultimate load stage for the tested beams. This may be due to the small amount of CFRP ratio used in the experimental work leading to a failure of sheets by similar levels of vertical loading. Also, it is clear that adopting any method of simulation for the CFRP elements has no significant effect on the results; thus one can simulate the CFRP sheet as LINK8 element for simplicity and reduced time of building of the model.

Prestress Effect Simulation

The analysis is performed using two load steps. The first one includes the application of prestress force. Then, the static load is applied as a second step. The prestress effect on the CFRP sheet has been expressed in two manners. In the first manner, the prestress is simulated by equally distributed axial load which in turn may be substepped. The other one is represented as an initial axial strain.

The difference in the results obtained due to

adopting the methods of the prestress effect simulations can be clearly seen. It is obvious that for low levels of prestress**,** good agreement with the experimental work can be seen when adopting any one of the two methods as shown in Figs. 12 and 13. However, Fig. 14 reveals that for relatively higher prestress level, some divergence may be obtained in the initial stages of loading when adopting the initial strain model.

The divergent solution for beam B4 in the early stage of loading may be attributed to that the application of a large amount of strain (which may not be accommodated by the structure immediately) may result in some inaccurate results (instability in the numerical solution). This inaccuracy in results cannot be seen obviously with relatively lower levels of initial strain (beams B2 and B3).

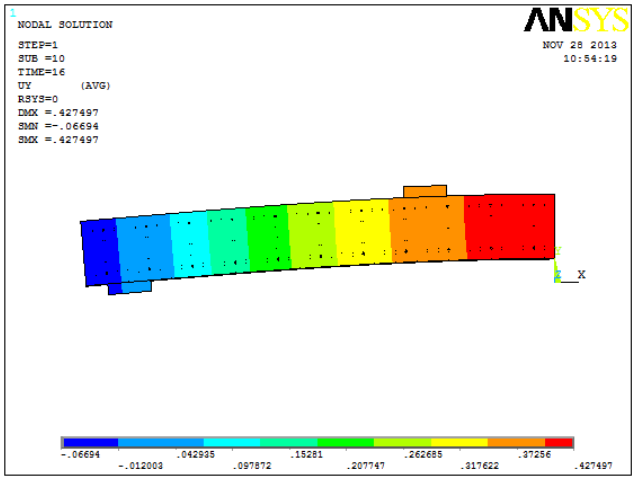

Figure (18): Camber for beam B3

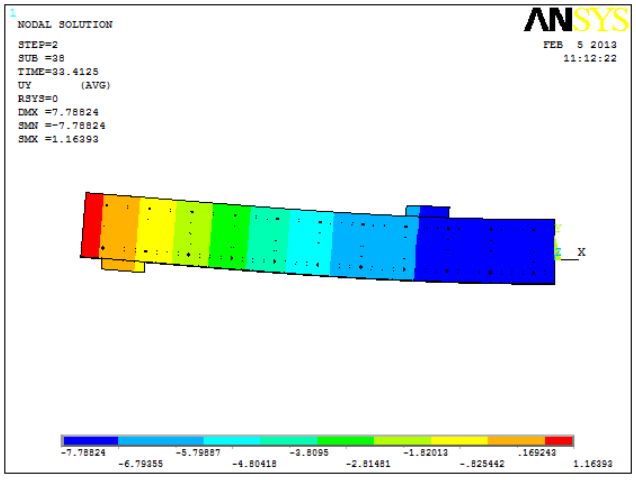

Figure (19): Deflection at load = 17.41 kN for B3

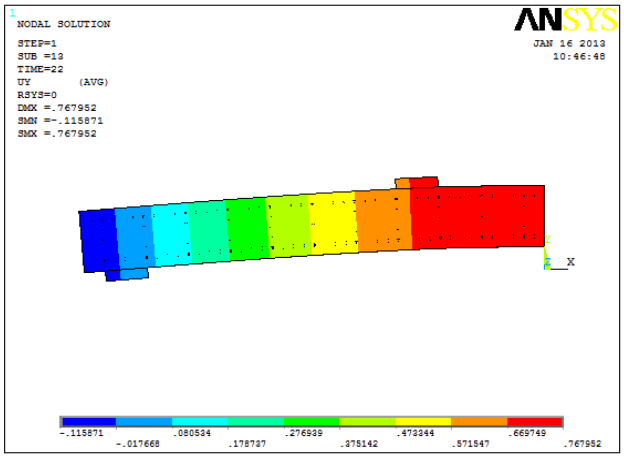

Figure (20): Camber for beam B4

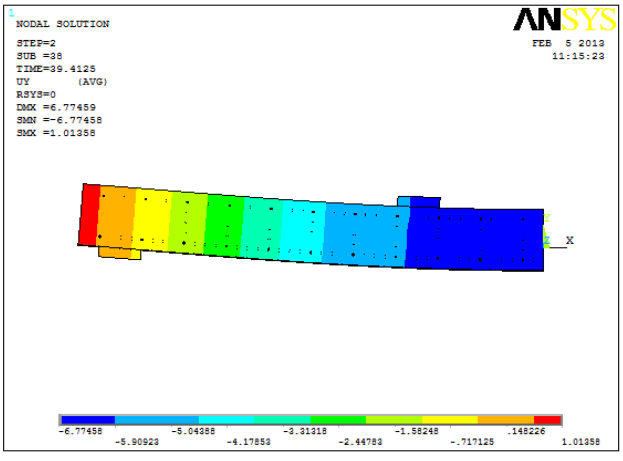

Figure (21): Deflection at load = 17.41 kN for B4

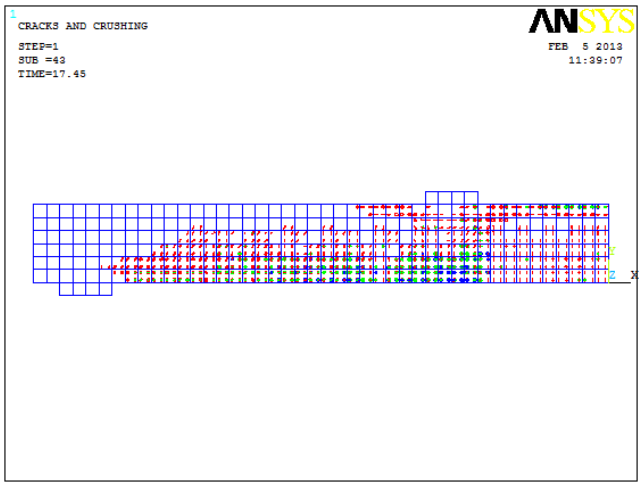

Figure (22): Crack pattern at load = 17.45 kN for B1

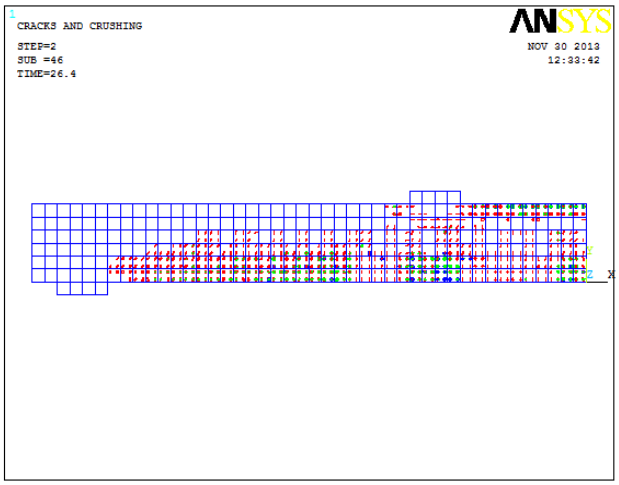

Figure (23): Crack pattern at load = 17.45 kN for B2

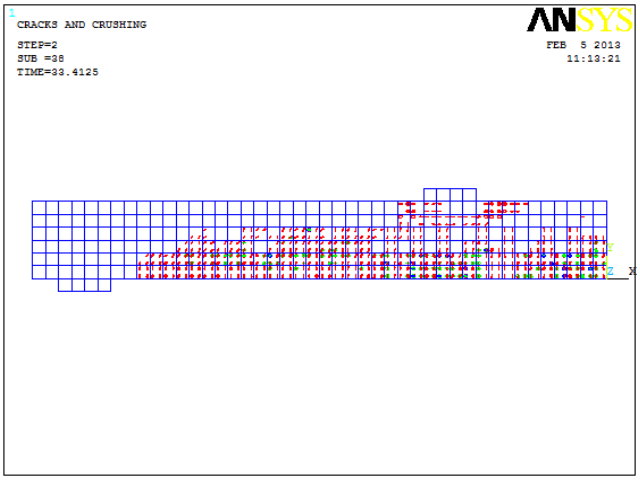

Figure (24): Crack pattern at load = 17.41 kN for B3

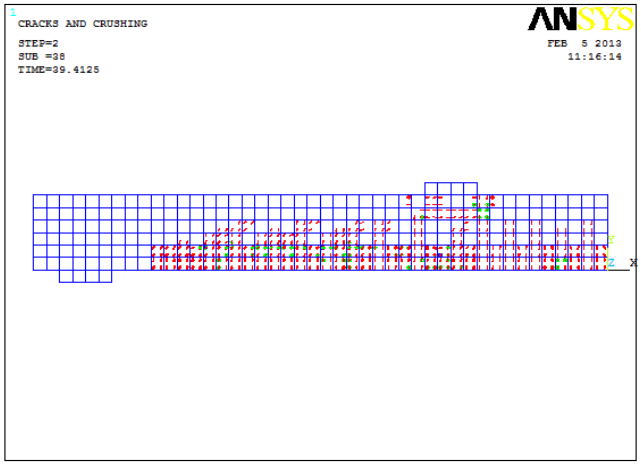

Figure (25): Crack pattern at load = 17.41 kN for B4

Effect of Prestress on Deflection and Crack Propagation

The effect of prestress value on response in terms of mid-span deflection and crack propagation has been studied, and the results are shown in Figs. 15 to 25. A vertical load level of about 17.45 kN has been chosen (the yield load of the control beam B1) to compare the results obtained from the numerical analysis for all beams.

For the deformed shape of the control beam B1, Fig. 15, the maximum mid-span deflection is 13.5 mm, whereas the corresponding value for beam B2, Fig. 17, is 9.3 mm. A reduction of about 31% can be noticed. This may be attributed to the camber (max. value is 0.25 mm) for beam B2 which occurred at the instant of prestressing, Fig. 16.

For beam B3, the effect of prestress can be seen more obviously. A mid-span camber of about 0.42 mm, Fig. 18, has been obtained. The deformed shape shown in Fig. 19 reveals that the mid-span deflection is reduced by 44% relative to the control beam.

A similar conclusion can be drawn for beam B4.

The results are shown in Figs. 20 and 21 at the instant of full prestress and the load 17.45 kN. A reduction in mid-span deflection of about 56% is obtained compared with the control beam B1.

The effect of prestressing on rate of crack formation is shown in Figs. 22 to 25 at the same load level (17.45 kN). For beam B1, Fig. 22, the cracks are developed and propagated up and toward the support, but in a rate greater than for the prestressed beams (B2, B3 and B4). This rate is found to be significantly reduced with the increase of prestress level, because the shear resistances clearly developed with prestress application.

CONCLUSIONS

1) It can be easily concluded that the finite element model adopted in the present study is efficient enough to simulate the behavior of reinforced concrete beams strengthened with CFRP sheets.
2) For the beams considered in this work, it can be seen that there is no significant difference in results found when adopting LINK8 element instead of SHELL41 to simulate the CFRP sheets. This may be useful in reducing time needed to build the model in ANSYS. However, this conclusion should be used with care for beams other than shallow wide beams.
3) At low level of initial prestress, no significant difference may take place when expressing the prestress as an initial strain rather than as an axial force. It is recommended to adopt the first method due to its simplicity. But, for relatively higher levels of prestress, it is found that adopting the axial force technique yields better results than the axial strain technique.
4) Increasing prestress results in some increase of cracking loads with a reduction in deflection (at the same loading level). It is found that the application of prestress force of 9 kN, 16 kN and 22 kN improved the cracking load by 57%, 106 % and 170%, respectively. Also, prestressing has a significant effect on the rate of crack propagation.

Symbols:

α_m	Tension stiffening factor
ε	Strain at stress f_c
ε_o	Strain at ultimate compressive stress $f`_c$
B1	Control specimen (beam with zero prestressing force)
B2	First prestressed specimen (beam with prestress force of 9 kN)
B3	Second prestressed specimen (beam with prestress force of 16 kN)
B4	Third prestressed specimen (beam with prestress force of 22 kN)
CFRP	Carbon Fiber Reinforced Polymer
E_c	Concrete elastic modulus (MPa)
$f`_c$	Compressive strength of concrete (MPa)
$f`_t$	Tensile strength of concrete (MPa)
f_c	Stress at any strain ε, (MPa)
FRP	Fiber Reinforced Polymer
f_u	Steel ultimate strength (MPa)
f_y	Steel yield stress (MPa)
EX	Modulus of elasticity (MPa)
PRXY	Poisson's ratio
ShrCf-Op	Shear transfer coefficients for an open crack

ShrCf-Cl	Shear transfer coefficients for a closed crack
UnTensS	Uniaxial tensile cracking stress (MPa)
UnComp	Uniaxial crushing stress (MPa)
BiCompS	Biaxial crushing stress (MPa)
HydroPrs	Uniaxial crushing stress under the ambient hydrostatic stress state (MPa)
UnTensrFac	Uniaxial crushing stress under the ambient hydrostatic stress state (MPa)
St TenC	Stiffness multiplier for cracked tensile condition
Tang Mod	Tangent modulus (MPa)

REFERENCES

ACI 440 (American Concrete Institute Committee 440). (2002). "Guide for the design and construction of externally bonded FRP systems for strengthening concrete structures". American Concrete Institute Committee 440, Farmington Hills, Michigan, 45 pages.

Anthony, J., and Wolanski, B.S. (2004). “Flexural behavior of reinforced and prestressed concrete beams using finite element analysis”. M.Sc. Thesis, 57 pages.

Clarke, J.L. (1993). “Alternative materials for the reinforcement and prestressing of concrete”. Blackie Academic and Professional (An Imprint of Chapman and Hall).

Desai, Y.M., Mufti, A.A., and Tadros, G. (2002). "User manual for FEM PUNCH, version 2.0". ISIS Canada.

Gangarao, H.V.S., Taly, N., and Vijay, P.V. (2007). “Reinforced concrete design with FRP composites”. CRC Press, 382 pages.

Hollaway, L.C., and Leeming, M.B. (2001). “Strengthening of reinforced concrete structures using externally-bonded FRP composites in structural and civil engineering”. CRC Press.

Nordin, H. (2003). ”Flexural strength of concrete strength with prestressed near surface mounted CFRP rods”. Licentaite Thesis, Lulea University of Technology, Sweden, 57 pages.

Peter F. Takács, and Kanstad, J. (2002). ”Strengthening prestressed concrete beams with carbon fiber reinforced polymer plates”. NTNU Report R-9-00, Trondheim, Norway.

SAS ANSYS 10.0. (2005). “Finite Element Analysis System”. SAS IP, Inc., U.S.A.

Shang, S., Zou, P.X.W., Peng, H., and Wang, H. (2005). ”Avoiding de-bonding in FRP strengthened reinforced concrete beams using prestressing techniques”. Proceedings of the International Symposium on Bond Behavior of FRP in Structures (BBFS 2005).

Willam, K.J., and Warnke, E.P. (1974). "Constitutive model for triaxial behaviour of concrete”. Seminar on Concrete Structures Subject to Triaxial Stresses, International Association of Bridge and Structural Engineering Conference, Bergamo, Italy, 174 pages.